Received: 29 May 2021 | Revised: 29 May 2021 | Accepted: 30 June 2021

DOI: 10.1002/maco.202112569

ARTICLE

Materials and Corrosion

Electrochemical corrosion parameters for active and passive reinforcing steel in carbonated and sound concrete

Muazzam G. Sohail[1] | **Stéphane Laurens**[2] | **Fabrice Deby**[2] | **Jean P. Balayssac**[2] | **Nasser Al Nuaimi**[1]

[1]Center for Advanced Materials, Qatar University, Doha, Qatar

[2]Laboratoire Materiaux et Durabilite des constructions (LMDC), UPS, INSA, Université de Toulouse, Toulouse, France

Correspondence
Muazzam G. Sohail, Center for Advanced Materials, Qatar University, Doha, P.O. Box 2713, Qatar.
Email: muazzam.ghous@qu.edu.qa

Abstract

The electrochemical corrosion parameters, such as corrosion potential, corrosion current density, and the Tafel constants are necessary inputs for the corrosion modeling in reinforced concrete. Literature shows large variability in their values, whereas the data are scarce for the carbonated concrete. This paper presents a range of corrosion parameters for the active steel in carbonated and the passive steel in noncarbonated concrete. Forty-eight singly reinforced concrete cylinders were cast, of which 24 were carbonated and the others were sound samples. Potentiodynamic polarization curves were obtained at three different scan rates and extrapolated to extract the corrosion parameters. To validate these parameters, a macrocell corrosion system was simulated using FEM-based Comsol multiphysics® software. The numerical results were compared to two experimental studies. A natural dispersion in the values of corrosion parameters for both active and passive steels was observed. The average Stern–Geary constant was 54 and 47 mV for active and passive steels, respectively. Numerical simulations with the obtained parameters predicted the macrocell corrosion in partially carbonated concrete with a high accuracy. The presented values of corrosion parameters in this study could help researchers and engineers to simulate the corrosion phenomena in concrete accurately.

KEYWORDS

carbonation of concrete, corrosion parameters, numerical modeling of corrosion, reinforcement corrosion in concrete, Tafel plots

1 | INTRODUCTION

Corrosion in reinforced concrete (RC) has become a significant cause of the deterioration of civil infrastructure and a massive burden on the global economy. Although, the concrete cover provides physical and chemical protection to the rebar thanks to its basic pH (~13), which enables a passive layer at reinforcement and hinders corrosion.[1,2] However, carbonation in concrete lowers the pH below 9, which destroys the passive layer and initiates the corrosion process. Corrosion initiation in RC structures takes several years, and the artificially

induced corrosion in the laboratory environment is very laborious and time-consuming. That is why the numerical tools to predict the corrosion propagation and the damage to RC structures are gaining much attention from the research and engineering community. Several mathematical models for the initiation and propagation phases are proposed to assess the damage and the remaining service life of RC structures.[3–5]

As corrosion is an electrochemical process, the models based on the electrochemical laws could simulate the corrosion on steel surfaces in concrete realistically. Butler–Volmer kinetics, Ohms' law, and charge conservation law are employed successfully to model steel corrosion in concrete in the propagation phase.[2,6–10] The Butler–Volmer relationship is essentially an algebraic sum of the rate of anodic and cathodic reactions, described in the following equation:

$$I_{\text{corr}} = i_{\text{corr}}\exp\left(\frac{\log(10)(E - E_{\text{corr}})}{\beta_{\text{a}}}\right) - \exp\left(\frac{-\log(10)(E - E_{\text{corr}})}{\beta_{\text{c}}}\right), \quad (1)$$

where, I_{corr} is corrosion current at a polarized potential E, i_{corr} is instantaneous corrosion current density at the equilibrium potential E_{corr}, and β_{a} and β_{c} are the anodic and cathodic Tafel slope constants, respectively. These entities are called electrochemical corrosion parameters. It is essential to input the precise values of these parameters as per the condition of steel and concrete in the model so that the corrosion current could be accurately predicted.

In addition, the linear polarization resistance (LPR), a commonly used corrosion measuring technique, employed an entity called Stern–Geary constant B. Its values are fixed to 26 and 52 mV for actively corroding and passive steel rebars, respectively. However, it depends on the anodic and cathodic Tafel constants and is required to be estimated for a given concrete and steel conditions.

The electrochemical corrosion parameters show variability and depend on the state of the steel rebars and the surrounding concrete. That is, whether the steel is in an active or passive corrosion state and whether the concrete is carbonated, chloride contaminated, saturated, or dry. Furthermore, the roughness of steel surface, oxide layer, concrete moisture content, pH of pore solution, presence of different ions in pores, and temperature also affect the corrosion parameters.[11,12] Moreover, the geometry of the sample also influences their values.[9] For these reasons, in reinforced concrete, the values of β_a and β_c could be very different (mostly higher) than normally employed values in the LPR technique or for numerical simulations.

The Butler–Volmer equation is set as the boundary condition on the steel–concrete interface to measure the corrosion rates during numerical simulation. It's parameters for active and passive steels in the available literature exhibit large variability.[2,6,7,13,14] For example, Warkus et al.[15] used β_{a} between 100 and ∞mV/dec for active and passive steel, respectively, whereas Redaelli et al.[10] employed β_{a} as 75 and 1000 mV/dec, respectively. Ge and Isgor[6] and Kim and Kim[16] employed 60 mV/dec for both anodic and cathodic Tafel slope constants for active steel. In most cases, these parameters are either assumed or obtained experimentally in simulated concrete pore solutions rather than in concrete.

Song[17] theoretically suggested that (i) if the steel is actively corroding and concrete is porous enough to allow sufficient oxygen such that the diffusion does not control the reduction reaction, the expected values of β_{a} are between 13 and 17 mV/dec, and β_{c} between 21 and 65 mV/dec. (ii) In the case where steel is in the active state, whereas the reduction reaction is diffusion controlled, the expected values of β_{a} are between 13 and 17, and β_{c} is ∞. (iii) When steel is in the passive state with enough oxygen availability to maintain the cathodic process, the β_{a} is ∞, and β_{c} is between 21 and 52 mV/dec. (iv) In the case, the steel is in a passive state and the cathodic reaction is also diffusion-controlled, both β_{a} and β_{c} are expected to be ∞.

Most of the experimentally obtained corrosion parameters are from chloride-contaminated concrete and show a wide range of values. Babaee and Castel[18] reported corrosion parameters on single rebar placed in a chloride-contaminated concrete. For actively corroding steels, the reported β_{a} values were between 430 mV/dec and infinity, whereas β_{c} was between 106 and 221 mV/dec. For passive steels, the β_{a} was infinity and β_{c} was between 30 and 45 mV/dec. Michel et al.[7] determined the corrosion parameters of active steel in chloride contaminated concrete prisms ($120 \times 130 \times 375$ mm). The experimentally measured corrosion current densities and corrosion potentials were modeled using Butler–Volmer kinetics at the steel surface, and the Tafel constants that gave the best fit were reported. The β_{a} for active steel was between 10 and 369 , whereas β_{c} was between 10 and 233 mV/dec, respectively. Garcés et al.[14] observed electrochemical corrosion parameters on an active steel bar in simulated concrete pore solutions of different pH. They found the corrosion potentials between −530 and −750 mV/SCE, anodic Tafel slope constant between 73 and 136 mV/dec, and cathodic Tafel slope constant between 112 and 242 mV/dec.

The steel-concrete interface conditions are different for chloride-contaminated concrete compared to carbonated concrete. Corrosion products are formed uniformly over the steel surface under carbonation, whereas the

chloride contamination results in pitting corrosion. Carbonated concrete offers higher resistance to ionic current than chloride-contaminated concrete. Hence, electrochemical corrosion parameters are expected to be dissimilar. Duprat et al.[19] reported the corrosion parameters in carbonated and noncarbonated concrete. The mean values of β_a and β_c, were 868 and 473 mV/dec for active steel in carbonated concrete, respectively, whereas, for the passive steel, the values were 637 and 218 mV/dec, respectively. These values also show a large offset from the generally employed values. Also, the anodic Tafel constants for active steel are higher than that of passive steel, which is the opposite compared to what is reported in other research works. Poursaee[20] experimentally found the anodic and cathodic Tafel constants in carbonated concrete as 247 and 466 mV/dec, respectively.

Limited literature is available on the electrochemical corrosion parameters in carbonated concrete. This study reports the naturally existing range of each corrosion parameter for active steel in carbonated and passive steel in noncarbonated concrete. The Stern–Geary constant for the LPR technique is also calculated from the generated data. A macrocell corrosion system of active and passive rebars in the partially carbonated concrete is numerically modeled to validate the measured range of corrosion parameters. The simulations are performed in the AC/DC module of the commercially available software COMSOL Multiphysics®. The values of macrocell corrosion current are compared against the experimental results presented in References [2,21]. The presented data on the corrosion parameters in carbonated concrete could be a valuable addition to the literature.

2 | EXPERIMENTAL DETAILS

2.1 | Sample geometry and materials

Forty-eight singly reinforced concrete cylinders of 65 × 130 mm dimensions were cast. The schematic of geometry and a cast sample is presented in Figure 1. Plain mild steel rebar with 20 mm diameter and 140 mm length was embedded at the center of the cylinder. A 20 mm length of the bar was kept outside the concrete for the electrical connection. The mill scale was removed from the steel surface by mechanical brushing. With the mill scale removed, all the bars are expected to corrode uniformly and behave similarly during electrochemical tests. The projected steel portion was covered with aluminum tape to prevent corrosion during carbonation. An epoxy layer was applied around the projected steel at the top surface of the cylinders to prevent CO_2 penetration through the steel-concrete interface.

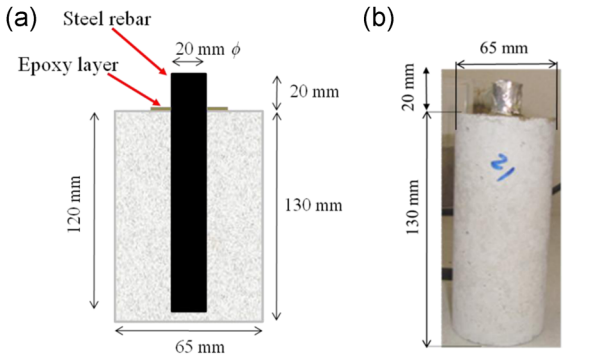

FIGURE 1 (a) Schematic of the sample geometry and (b) a concrete cylinder with embedded steel rebar [Color figure can be viewed at wileyonlinelibrary.com]

TABLE 1 Composition of mild carbon steel rebars, as provided by the manufacturer (wt%)

C	Si	Mn	P	S
0.45	0.3	0.7	0.035	0.035

A concrete cover of 22.5 mm circumferentially and 10 mm at the bottom of the steel was provided. Selected cylindrical geometry allows uniform polarization of the whole surface of steel rebars. In addition, the error in the estimation of the polarized area is eliminated.

Table 1 presents the chemical composition of the steel. Table 2 presents the concrete mixture proportion. Ordinary Portland cement CEM I 52.5R, washed sand of 0/4 mm, and coarse aggregates of 4/10 mm were employed. The carbonation rate in a normal strength concrete is between 1 and 8 $mm/\sqrt{year}$.[22] The carbonation front takes several years to reach the steel-concrete interface, even with a smaller cover thickness. A higher water-to-cement (w/c) ratio increases the carbonation rate.[23] That is why to reduce the experimental time, concrete with a higher w/c ratio of 0.78 was employed.

2.2 | Conditioning

Samples were cured under 100% relative humidity for 28 days. Twenty-four (24) samples were placed in a carbonation chamber set at 50% CO_2, 65% RH, and 23°C temperature. The other 24 cylinders were kept in a controlled laboratory environment at 23°C. Five reference samples were also placed in the carbonation chamber. These samples were broken at regular intervals to monitor the carbonation depth by spraying the phenolphthalein on the broken surface. If the pH of the concrete pores is above 11, the phenolphthalein spray changes the color of the concrete surface to pink, as shown in Figure 2a, whereas the carbonated concrete yields no change in color as the pH is dropped below 9.

TABLE 2 Concrete mixture proportion

Cement (kg/m^3)	Sand 0/4 mm (kg/m^3)	Gravel (4/12.5 mm) (kg/m^3)	Water (kg/m^3)	Water-to-cement ratio
280	854	1068	218	0.78

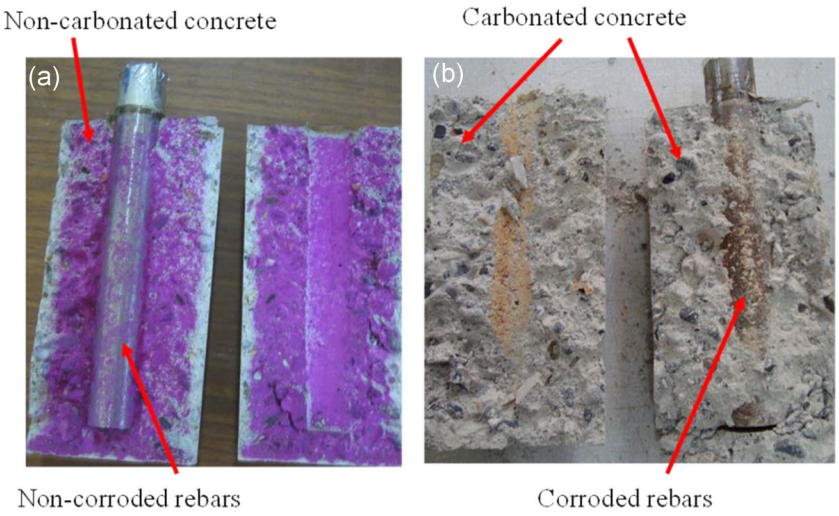

FIGURE 2 (a) Noncarbonated sample, phenolphthalein spray gave pink color indicating no carbonation, and (b) carbonated cylinders after conditioning, phenolphthalein spray became colorless, steel rebar was uniformly corroded [Color figure can be viewed at wileyonlinelibrary.com]

Figure 2a shows a noncarbonated sample after 10 weeks under laboratory conditions. The concrete surrounding the steel had a pink color, whereas the steel rebar was in a pristine state with no corrosion. Figure 2b shows a carbonated sample; the concrete cover was fully carbonated in 10 weeks. The steel surface was uniformly corroded.

2.3 | Testing setup and testing matrix

The potentiodynamic Tafel polarization of ±200 mV was applied using the DC module of the Gamry® potentiostat. Figure 3 schematically presents the three-electrode setup, consisting of a working electrode (WE), a counter electrode (CE), and a reference electrode (RE). The WE was the embedded steel rebar, CE was a titanium mesh, and saturated calomel electrode (SCE) was the RE. The CE was wrapped around the concrete cylinders so that the steel surface is uniformly polarized. Samples were kept in a quasi-saturated state during the experiments to eliminate the humidity effects on the reading. In addition, 2 cm of the sample were kept out of water for sufficient oxygen supply during the electrochemical measurements, as depicted in Figure 3. The experiments were carried out at 23°C ± 3°C.

Table 3 presents the testing matrix. Three scan rates of 0.1, 0.5, and 0.8 mV/s were applied to obtained Tafel plots. Six samples from both types of concrete were tested at each scan rate to present a statistical comparison and remove human error and material defects. The faster scan rates minimize the experimental time; however, the

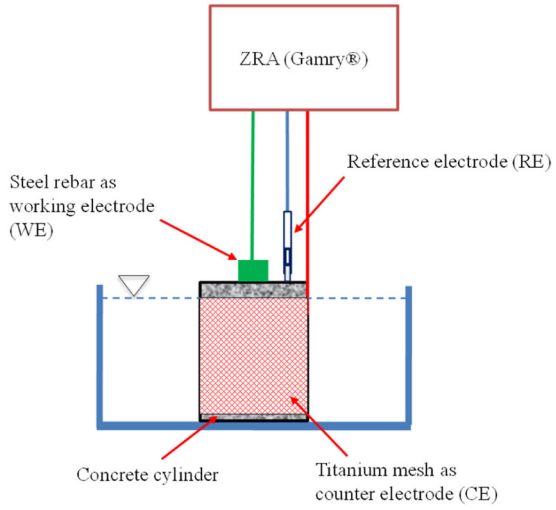

FIGURE 3 Three-electrode setup for the potentiodynamic polarization curves [Color figure can be viewed at wileyonlinelibrary.com]

electrochemical system is disturbed, the steady-state condition is not allowed during the application of each polarization step. Therefore, it might result in an overestimation of corrosion current densities. On the contrary, a slower scan rate ensures steady-state conditions, but it alters the ionic concentration around the electrode surface affecting the corrosion kinetics and the shape of polarization curves. Nevertheless, the selected scan rates are frequently used by researchers.[20,24–26]

The OCP was measured against SCE for 30 min, so that it becomes steady, and then the Tafel polarization of

TABLE 3 Testing matrix for the carbonated and noncarbonated concrete samples at different scan rates

Polarization type	Polarization swap	Scan rate (mV/s)	Noncarbonated sample	Carbonated sample
Potentiodynamic cyclic polarization	−200 mV to OCP to +200 mV	0.1	6	6
		0.5	6	6
		0.8	6	6
Anodic polarization	+200 mV to OCP	0.5	3	3
Cathodic polarization	−200 mV to OCP	0.5	3	3
Total = 48			24	24

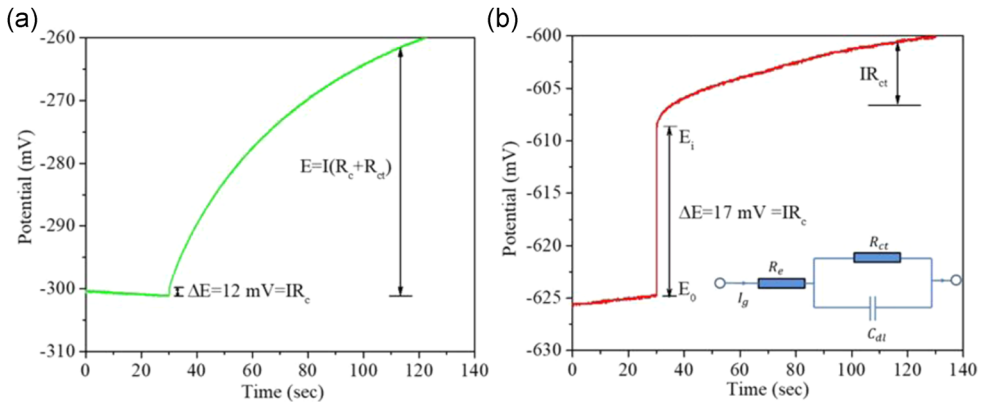

FIGURE 4 Response to a galvanic pulse of 50 μA of (a) noncarbonated and (b) carbonated cylindrical concrete sample. Randles equivalent circuit is shown in (b) [Color figure can be viewed at wileyonlinelibrary.com]

±200 mV was applied. The potentiodynamic scan started from −200 mV to OCP, then continued from OCP to +200 mV. The selected range of applied polarization is reported in the literature.[27–30]

The swap direction affects the corrosion potential and the slope of the anodic/cathodic branches. For example, if the swaps start from +200 mV, that is, the anodic polarization, the corrosion potential, E_{corr}, shifts toward the positive values than OCP, whereas, when it starts from −200 mV, that is, the cathodic polarization, the E_{corr} shifts toward a negative value than OCP. The partial anodic or cathodic polarization was applied to three carbonated and noncarbonated samples each (refer to Table 3) to observe their impact on corrosion parameters.

2.4 | Ohmic drop (IR) compensation

The electrical resistance of concrete causes an IR of potential between the CE and WE; that is, a portion of the applied potential is lost during the polarization. Hence, the potential applied at the concrete surface through CE is not equal to the one polarizing the steel surface. As Tafel plots are log (I) ~ E curves, to extract the corrosion parameter accurately, it is essential to know the exact value of the polarizing potential. This necessitates the IR compensation before extracting corrosion parameters. The IR compensation was carried out manually on log(I) ~ E data by measuring the concrete resistance (R_c). The galvanostatic pulse technique was used to measure the concrete resistance. A pulse of 50 μA was applied to cylindrical samples through CE and the responses of concrete and steel rebar were observed. Figures 4a and 4b, respectively present the response of noncarbonated and carbonated samples to the applied galvanostatic pulse. The E_0 is the initial potential of rebar, before the application of the galvanic pulse, E_i is the potential immediately after the pulse was applied.

The concrete resistance was calculated using Equation (2). The equation represents the Randles circuit model depicted in Figure 4b. The concrete cover acts as an electrolyte and offers resistance, R_c to the applied current. This resistance is in series with Faraday's process at the electrode surface, that is, the charge transfer resistance (R_{ct}) (polarization resistance) and the double-layer capacitance (C_{dl}). The R_{ct} and C_{dl} are parallel to each other.

$$\frac{\Delta E}{\Delta I} = R_c + \left(1 - e^{-\frac{t}{R_{ct}C_{dl}}}\right)R_{ct}. \quad (2)$$

Immediately after the pulse is applied, at the time, $t = 0$, the second part of Equation (2) is eliminated and R_c

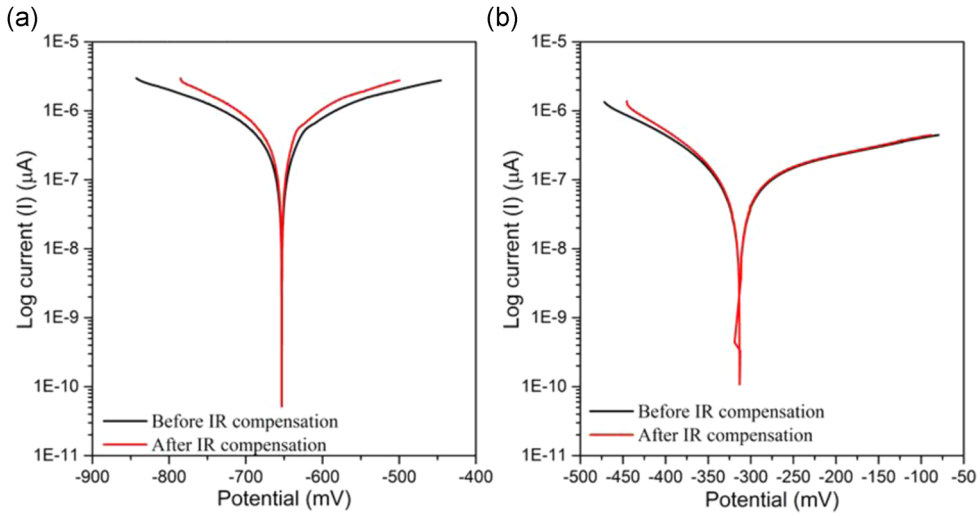

FIGURE 5 Polarization curve of (a) carbonated and (b) noncarbonated concrete samples with and without ohmic drop (IR) compensation [Color figure can be viewed at wileyonlinelibrary.com]

is obtained. At $t = \infty$, the exponent term becomes zero, and R_c plus R_{ct} are obtained as illustrated in Figure 4a,b. When the pulse is applied, the potential shifts vertically upward. The rise in potential represents the ohmic drop due to the concrete. Then the curve starts having an arc shape, which becomes flat with time. This portion is the polarization resistance of the steel rebar. The behavior of active and passive steels was distinctly different under the applied galvanic pulse. Passive steel showed a higher increase in potential response compared to active steel.

The R_c was 250 and 340 Ω for noncarbonated and carbonated concrete, respectively. The higher resistance in carbonated concrete was due to the calcium carbonates filling the concrete pores. As a result, the porosity is reduced, and the electrical resistance is increased. Once the concrete resistance was known, the ohmic compensation was applied, according to the below equation:

$$E_{\text{corrected}} = E_{\text{measured}} \pm \text{IR}_c. \quad (3)$$

Figure 5 presents the polarization curves with IR compensation. A positive correction was applied to the cathodic branch and a negative correction to the anodic branch. As the R_c is higher in the carbonated samples, the IR compensation effects are significant, and the curves showed higher slopes in the Tafel regions (Figure 5a). The IR compensation had an insignificant effect on the polarization curves of the noncarbonated samples (Figure 5b).

2.5 | Extrapolation of the curves

Figure 6 demonstrates the extrapolation of the IR-compensated Tafel plots. The linear branches are extending until the E_{corr}. The point where these extended

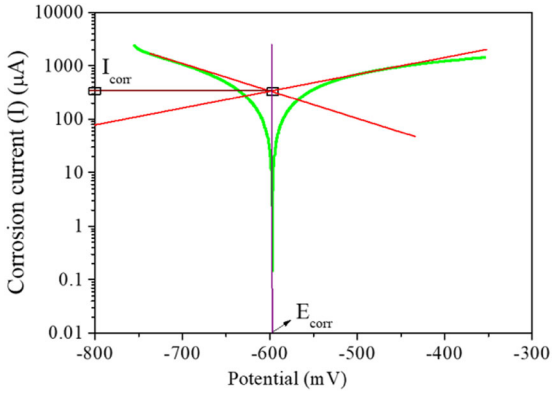

FIGURE 6 Tafel extrapolation; a vertical line is drawn at E_{corr} and the linear branches are then extended till this vertical line. Their intersection is the corrosion current density. The slopes of the extended lines are Tafel constants [Color figure can be viewed at wileyonlinelibrary.com]

lines intersect the vertical line on E_{corr}, is the value of corrosion current, I_{corr}. The slopes of these lines are the Tafel slope constants.

3 | RESULTS AND DISCUSSION

3.1 | Corrosion potential

Figure 7a shows the scatter of the corrosion potential values at active steel $E_{corr,a}$ in the carbonated concrete, through the box-plot distribution. The values suggest that the rebars were depassivated, and microcell corrosion activities were ongoing. The values were in the range between −543 and −702 mV/SCE. The average value was −652 mV/SCE

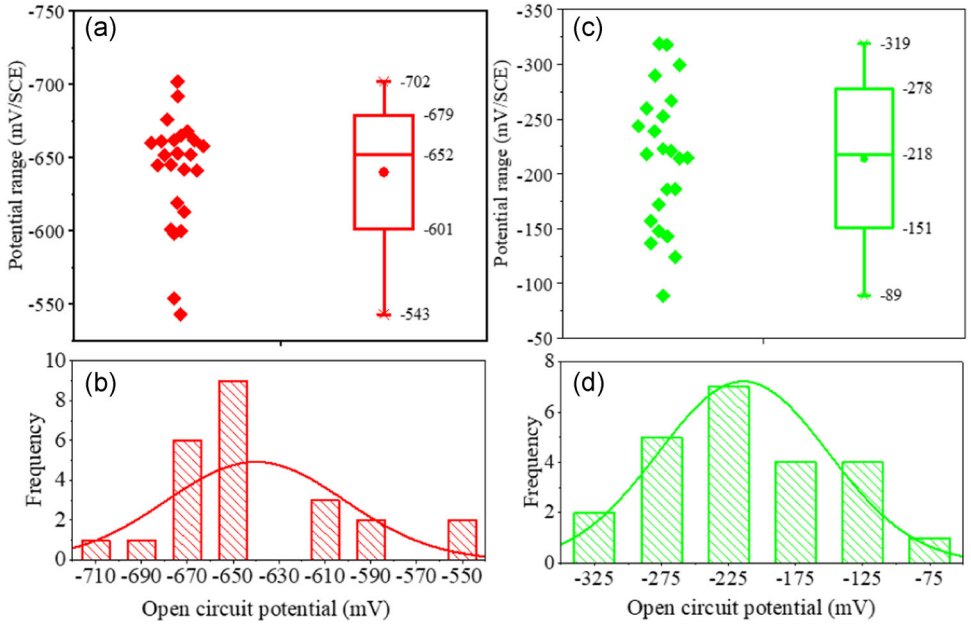

FIGURE 7 (a) Corrosion potential distribution and (b) histogram classes on the active steel in carbonated, and (c,d) are potential spread and histogram for passive steel in noncarbonated concrete samples, respectively [Color figure can be viewed at wileyonlinelibrary.com]

with a standard deviation (*SD*) of 38 mV/SCE. Figure 7b shows the histogram of the corrosion potential's values, the most frequently occurring class was −650 mV/SCE. The range observed here agrees with the available literature on half-cell potential (HCP) values for actively corroding steel in concrete.[9,31] The ASTM C876-09[26] standard suggests that with HCP below −426 mV/SCE, there is a 90% probability that the corrosion is initiated.

Figure 7c presents the statistical distribution of the corrosion potential for passive steel rebars, $E_{corr,p}$, in noncarbonated concrete samples. The values were between −143 and −319 mV/SCE over 24 samples, with an average of −240 mV/SCE, and an *SD* of 48 mV/SCE. The most frequent class of potential values in the histogram was −225 m/SCE (shown in Figure 7d).

The $E_{corr,a}$ values are clustered around the average and the mean values. If the two extreme values are ignored in Figure 7a, the dispersion is not significant. The 15 out of 24 samples were in two classes of −650 to −670 mV/SCE on the histogram. On the contrary, $E_{corr,p}$ showed larger variability, this observation has already been reported and explained by researchers.[9,20] Its values fluctuate depending upon the moisture contents and the oxygen availability inside the concrete.[32] A dry concrete could generate higher potential (positive) values, indicating less or no corrosion activities even on active steel, whereas, in wet concrete with oxygen-deprived steel surfaces, the measured potential values could be lower (negative).

Theoretically, the corrosion potential is a point where anodic and cathodic current densities are at equilibrium. Graphically, it is the point where anodic and cathodic branches intersect on a linear scale polarization curve. As a noncorroding metal remains passive for a large range of potential values and produces lesser current during polarization, that is why its anodic branch mostly remains a straight line parallel to the potential axis on the polarization curve. The point where the cathodic branch intersects the anodic branch depends on the oxygen availability on the cathode site. On the basis of the concrete conditions, the equilibrium point could move up and down on the potential axis. That is why a more negative corrosion potential (up to −300 mV/SCE) on the passive steel is not necessarily an indication of corrosion initiation. Bertolini et al.[33] suggested that the dispersion of corrosion potential depends on the concrete pores' conditions, the types of ions it contains, and its pH values since higher pH (~13) helps to form and stabilize oxide layers. Soleymani and Ismail[34] reported that once the concrete is saturated (higher RH), the measured corrosion potential drops to more electronegative values even though corrosion rates are not increased. Hence, the measured potential values could be anywhere between +100 and −350 mV/SCE for passive steel in concrete.

3.2 | Corrosion current density

Figure 8a presents the distribution of corrosion current densities on the active steels, $i_{corr,a}$, in the carbonated concrete. The values were in a range between 0.3 and

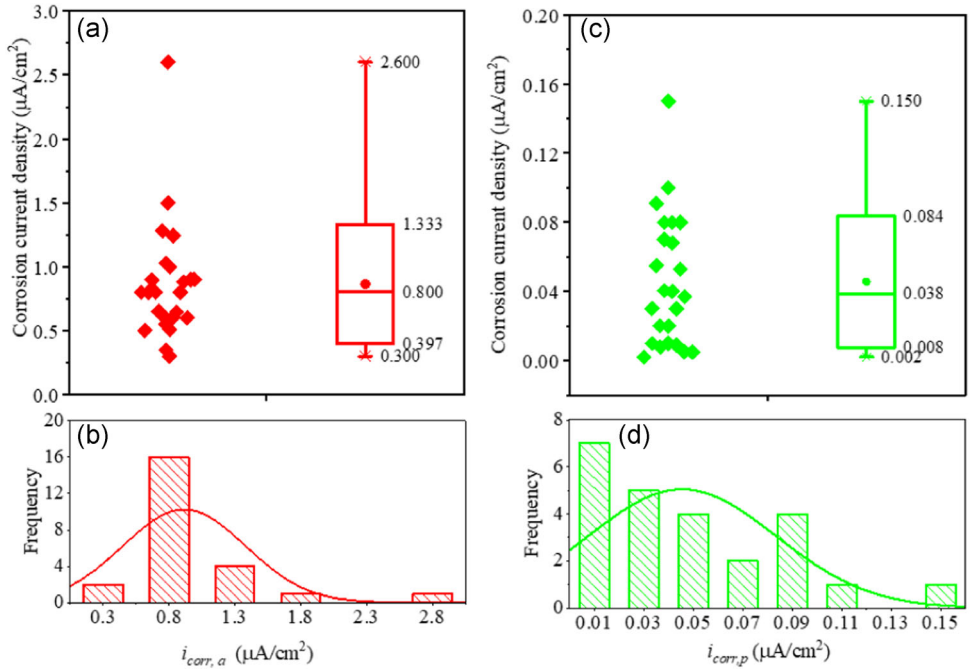

FIGURE 8 Corrosion current density distribution of steel rebars in (a,b) carbonated and (c,d) noncarbonated concrete samples [Color figure can be viewed at wileyonlinelibrary.com]

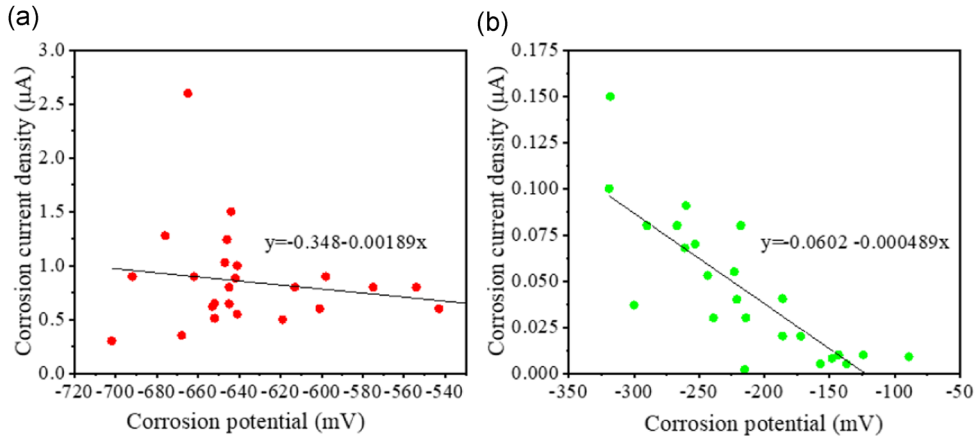

FIGURE 9 Corrosion current versus potential relation for (a) active steel in carbonated and (b) passive steel in noncarbonated samples [Color figure can be viewed at wileyonlinelibrary.com]

2.60 μA/cm² over 24 samples. With an average of 0.903 μA/cm², a median of 0.88 μA/cm², and *SD* of 0.516 μA/cm². Figure 8b shows the statistical histogram of $i_{corr,a}$, the most frequent class was 0.8 μA/cm². Sixteen samples were in the range from 0.5 to 1 μA/cm². These values illustrate very high corrosion rates on the steel surface.[17]

Figure 8c presents the corrosion current densities on the passive steel rebars, $i_{corr,p}$, in noncarbonated concrete. The values scattered between 0.01 and 0.15 μA/cm², with an average of 0.058 μA/cm², a median of 0.05 μA/cm², and an *SD* of 0.034 μA/cm². The most frequent classes on the histogram were 0.01 and 0.02 μA/cm². Sixteen out of 24 samples showed values less than 0.05 μA/cm². Only two samples had corrosion current higher than 0.1 μA/cm².

Thus, the active steel in carbonated concrete had 10–15 times higher corrosion current densities than the passive steel in noncarbonated concrete. The partially polarized samples showed similar current density ranges as measured at samples polarized for a complete cycle of polarization.

Figure 9 illustrates the corrosion current densities versus the corrosion potentials relationship. More electronegative potentials are supposed to produce higher

corrosion rates. However, with more electronegative potentials the currents were not necessarily increased on active steel in carbonated concrete. This could be attributed to the rust products formed on the steel surface which hinder the mobility of Fe^{2+} ions to move away from the steel surface to react with OH^- ions. This creates a positive charge barrier near the steel surface, which resists the extraction of electrons during anodic polarization, resulting in lower corrosion currents even at higher potentials. In addition, the potential values are sensitive to moisture contents, pore solution, and concrete resistivity. The HCP measurements are a qualitative indication of corrosion, and their values may not correlate to the corrosion rate on steel surfaces. This observation has been reported by several researchers.[2,3,9,20,27]

Figure 9b shows the corrosion versus potential relationship of the passive steel rebars. It could be observed that the current was not increased with more electronegative potentials. The potential values are dependent on the anodic and cathodic reaction rates. The reduction reaction rate is higher in noncarbonated samples due to the abundant availability of oxygen, which could shift the corrosion potential to electronegative values and also result in slightly higher corrosion current densities on the Tafel plots. Some researchers reported the limit of corrosion potential to be above −140 mV/SCE; however, as shown in this study, the passive potential could be up to −300 mV/SCE.

3.3 | Anodic and cathodic Tafel constants

In the case of anodic and cathodic Tafel slope constants, a more significant discrepancy is reported in the literature, for example, anodic Tafel slope constants for active steel, $\beta_{a,a}$, has been reported between 8 and 2100 mV/dec.[19,20,27] They vary naturally depending on the rebar conditions, passive layer, and concrete pore solution. That is why some researchers proposed to refer to them as Tafel coefficients rather than Tafel constants.[27] Figure 10a demonstrates the distribution of $\beta_{a,a}$ in carbonated concrete. The values were dispersed over a range between 180 and 280 mV/dec. The average value over 24 samples was 244 mV/dec, and the standard deviation was 28 mV/dec. Figure 10b shows the statistical histogram classes of $\beta_{a,a}$ in carbonated concrete. The frequently occurring class was 250 mV/dec. Nguyen et al.[35] reported a mean value of $\beta_{a,a}$ as 180 mV/dec with a coefficient of variance of 22.4%. Poursaee[16] found values of $\beta_{a,a}$ of 247 mV/dec in carbonated concrete. These values are very close to the ones found in the present study. However, Duprat et al.[19] reported a mean value of $\beta_{a,a}$ of 868 mV/dec in carbonated samples, these values are very high considering the active corrosion state of steel rebars. The geometry of the samples in the case of Duprat et al.[19] was very different than what is employed in this study. They reported the parameters on steel rebar

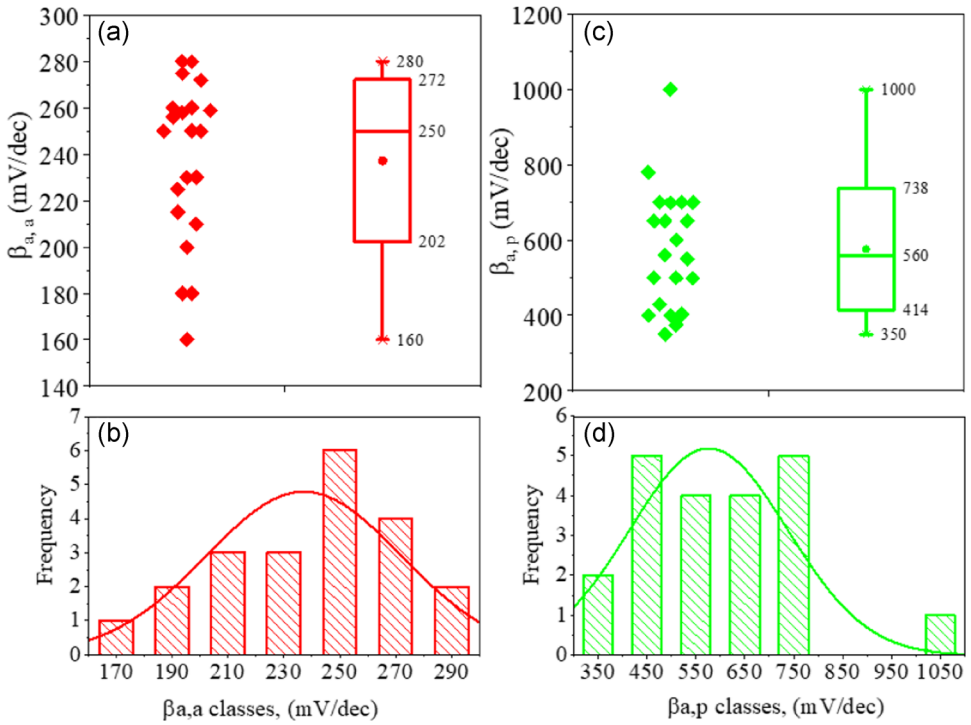

FIGURE 10 Statistical distribution of anodic Tafel slope constant for (a) scatter on active steel and (b) passive steel, (c,d) histograms of distribution for active and passive steels, respectively [Color figure can be viewed at wileyonlinelibrary.com]

embedded in block samples, such geometry does not allow for uniform polarization of the whole steel surface. Moreover, the concrete mixture, cement, aggregates, and concrete resistivity were all different. These aspects could influence polarization behavior.

Figure 10c presents the values of the anodic Tafel slope constant of passive rebars, $\beta_{a,p}$, in sound concrete. The values were between 350 and 1000 mV/dec with an average of 560 mV/dec and an *SD* of 129 mV/dec. The values were more dispersed compared to the values of $\beta_{a,a}$. The anodic reactions are sluggish in passive steel due to higher polarization resistance; the current is not increased with an increase in polarizing potential, resulting in a flat anodic Tafel branch. The straight line drawn on it would require a higher number of mVs to cross one decade on the logarithm scale and renders a very high value of $\beta_{a,p}$. Usually, the $\beta_{a,p}$ values are higher than $\beta_{a,a}$. Several researchers have employed it as infinity while modeling the macrocell corrosion due to its insignificant influence on the macrocell corrosion system after a specific value (i.e., ~700 mV/dec).[2,6,9,15,27]

Figure 11a presents the distribution of cathodic Tafel slope constants for the active steel rebar, $\beta_{c,a}$, in carbonated concrete. The values were between 190 and 350 mV/dec with an average value of 240 mV/dec and *SD* of 39 mV/dec. Figure 11b depicts that the most frequent class on the histogram was 230 mV/dec. Fifteen out of 24 samples were between 230 and 290 mV/dec. Theoretically, $\beta_{c,a}$ should be higher than $\beta_{a,a}$ in carbonated concrete, as oxygen reduction rates at cathodes are expected to be lower than the iron oxidation. This is because of the lack of available oxygen as the concrete pores are filled with calcium carbonate once the carbonation process is occured. Moreover, as the steel rebar corrodes uniformly under carbonation attack, fewer cathodic sites are available to allow oxygen reduction once the complete surface is corroded. This tendency was observed in this study, however, the difference between $\beta_{a,a}$ and $\beta_{c,a}$ was not as significant as has been reported in the literature.[20,21,27] In this study, quasi-symmetric polarization curves were observed in carbonated concrete, and the anodic and cathodic slopes were nearly identical. This could be attributed to ample oxygen availability. This oxygen availability is due to the higher w/c of 0.78, which resulted in 15% porosity even after concrete carbonation. Some studies also showed that the $\beta_{c,a}$ on active steel in chloride-contaminated concrete has lower values than $\beta_{a,a}$, implying that the reduction rate is higher and the corrosion system is not diffusion-controlled.[9,20]

Figure 11c illustrates the distribution of cathodic Tafel constant for steel ($\beta_{c,p}$) inside a noncarbonated concrete. Its values were between 105 and 180 mV/dec with an average of 136 mV/dec and *SD* of 21 mV/dec. The most frequent classes on the histogram were 150 mV/dec. Eighteen out of 24 samples were in classes 110 to 150 mV/dec. Its values were lower than the $\beta_{a,p}$, suggesting that the reduction rates of oxygen are higher compared to the oxidation of iron under applied polarization. Its values were also lower than the $\beta_{c,a}$, which means higher oxygen reduction on passive steel in sound

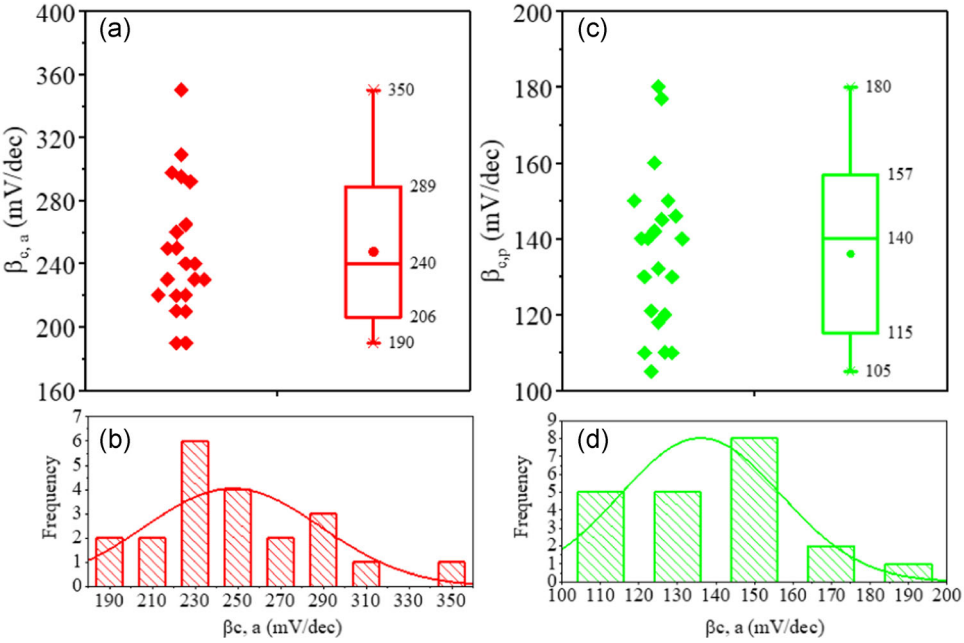

FIGURE 11 Statistical distribution of cathodic Tafel slope constant for (a) active steel and (b) its histogram distribution, and (c,d) are the values of passive steel [Color figure can be viewed at wileyonlinelibrary.com]

concrete compared with active steel in carbonated concrete. This could be attributed to the sufficient oxygen availability due to the higher porosity of noncarbonated concrete. Moreover, since no corrosion products are formed on passive steel, a higher surface area is available for oxygen reduction reaction during cathodic polarization. In the available literature, the values of cathodic Tafel constant in active and passive steel rebars are considered equal. This study shows that this is not the case, especially when the carbonated and noncarbonated concretes are under study.

3.4 | Stern–Geary constant

The LPR (R_p) technique is the most commonly used corrosion measuring technique, it is explained in Equation (4). To obtain i_{corr}, the (R_p) is related to Stern–Geary constant B as per Equation (5). In turn, the constant B is dependent on the anodic and cathodic Tafel slope constants, as per Equation (6).[17]

$$R_p = \frac{\Delta E}{\Delta I}, \tag{4}$$

$$i_{corr} = \frac{B}{R_p}, \tag{5}$$

$$B = \frac{\beta_a \times \beta_c}{2.303(\beta_a + \beta_c)}. \tag{6}$$

The guidelines to measure i_{corr} adopt the values of B as 26 and 52 mV for active and passive steels, respectively. For B to be equal to 26 mV, β_a and β_c should necessarily be 120 mV/dec, whereas, for B to be equal to 52 mV, β_a needs to be infinite and β_c to be 120 mV/dec. These values are recommended based on the study carried out by Andrade and González[34] on steel bars in a mortar and in $Ca(OH)_2$ solution. The values are extensively employed in the corrosion rate measurements by LPR on real RC structures. However, with these values, an error in the order of magnitude two could appear in the measured corrosion rates.[9,19,20] The values do not hold for several conditions of steel and concrete, such as uniform or pitting corrosion, carbonated or sound concrete, and dry or saturated concrete.

Figure 12a,b presents the statistical distribution of the calculated Stern–Geary constant B for active steel in carbonated and passive steel in nonconcrete, respectively. The values were calculated from the Tafel constants. For active steel rebars in carbonated concrete, B values were in the range between 40 and 68 mV with an average of 54 mV and an *SD* of 7 mV. Although for passive steel rebar in noncarbonated concrete, the values were in the range between 37 and 63 mV, with an average of 47 mV and an *SD* of 6 mV. The values of B for both active and passive steel bars are relatively close to each other, and there is an apparent overlap in their values. The average value in the case of passive steel was very close to those employed in the LPR technique to obtain the corrosion current densities, that is, 52 mV,[17] whereas, for active steel rebars, the values were two times higher than the recommended values of 26 mV. These recommendations assume much lower values of anodic and cathodic Tafel slope constants for the active steel in concrete.

The values of 26 and 52 mV were selected by Andrade and González[34] as these values matched the corrosion rates obtained with gravimetrical weight losses. However, the resistance of the carbonated concrete is higher than that of chloride-contaminated concrete and the simulated pore solutions. Therefore, the corrosion kinetics would be slower in the carbonated concrete. Hence, the values of the Tafel slopes are expected to be higher. Several researchers have already documented the observations made in this study on the Stern–Geary constant. This aspect of corrosion measurement techniques requires due intention from researchers and engineers so that the amount of damage is assessed accurately during the calculations of the remaining service life of RC structures.[20,27,36]

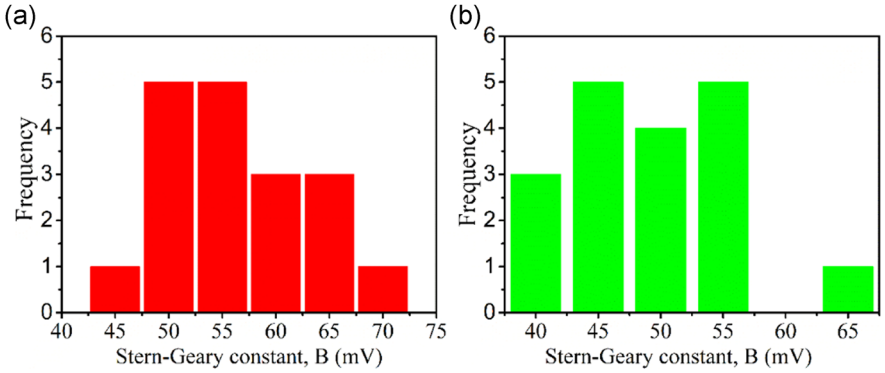

FIGURE 12 Stern–Geary constant values for (a) active steel in carbonated concrete and (b) passive steel in noncarbonated concrete [Color figure can be viewed at wileyonlinelibrary.com]

3.5 | Effects of scan rate

Tables 4 and 5 summarize all the parameters extracted from complete-cyclic potentiodynamic polarizations at three applied scan rates. Alongside other corrosion parameters, the Stern–Geary constant is also presented for all the samples. The tables also show the results of partial polarization scans. It was observed that the partial polarization yielded similar ranges of corrosion parameters.

Scan rates of the applied polarization could affect the corrosion current density and anodic and cathodic Tafel constants. The OCP is independent of scan rate, whereas the E_{corr} might offset from the initial OCP with higher scan rates. It shifts the polarization curves toward negative or positive values depending upon the start-point of the potential swap. An average offset of 13 mV between OCP and E_{corr} during Tafel polarization was observed. However, the offset values were not affected by the change in scan rate. The corrosion current densities also showed no variation in the samples tested under three scan rates in this study, and the values were overlapping (Table 4). The average value of corrosion current density for the carbonated samples tested at scan rates of 0.1, 0.5, and 0.8 mV/s were 0.62, 1.15, and 0.95 $\mu A/cm^2$, respectively. In noncarbonated concrete samples, the average corrosion current densities were 0.038, 0.073, and 0.064 $\mu A/cm^2$, respectively. Tafel slope constants were also not affected by the three selected scan rates applied in this study.

It is reported that the faster scan rate could result in a flat anodic branch of the polarization curve over a wide range of potentials.[18,37] Hence, the extrapolation could overestimate β_a and i_{corr} values. This behavior was observed when the scan rate was increased from 0.1 to 0.5 mV/s; however, reverse happened from 0.5 to 0.8; at 0.8 mV/s, the corrosion current values were higher than those with 0.1 mV/s. Babaee and Castel[18] observed that with higher scan rates, the corrosion current is overestimated, whereas the R_p values are underestimated. Martínez and Andrade[36] investigated the effects of changing scan rates from 0.001 to 83 mV/s on the corrosion current density. It was observed that starting from the lowest scan rate of 0.001 to a value of 0.17 mV/s, the R_p and i_{corr} were not affected; however, for a 0.17 mV/s scan rate till 2 mV/s, the R_p decreased and i_{corr} increased by many folds, and then become stable again on higher scan rate values. The used scan rates in this study are the most commonly employed ranges and do not significantly affect the polarization behavior and the corrosion parameters.

3.6 | Numerical modeling using obtained parameters

The carbonation in an RC structural member initiates from the outer surface while the inner concrete remains noncarbonated. As a result, the steel reinforcement in the carbonated portion becomes active, whereas, in sound concrete, it remains passive. Although the carbonation causes uniform corrosion on the active steel surface; however, galvanic/macrocell corrosion is established between active and passive steel due to their electrical connection. The weight and the cross-sectional losses on the active steel are several times higher under macrocell than under microcell corrosion. The rate of macrocell corrosion depends on the state of both steel rebars, their corrosion current densities, and the potential difference between them. Hence, the parameters of the active and passive steel affect the macrocell system.

To validate the presented range of corrosion parameters and demonstrate the importance of obtaining them accurately, a macrocell corrosion system in concrete was modeled numerically. Commercially available FEM-based software COMSOL Multiphysics® was used for these simulations. Figure 13 shows the geometry employed for the model. Active steel rebar is embedded inside a carbonated concrete cylinder, whereas passive steel is embedded in noncarbonated concrete, surrounding the inner concrete cylinder coaxially. The steel diameter was set as 20 mm, and the embedded length was 120 mm, as was the case of experimental samples in this study. The active and passive bars were placed at a distance of 65 mm c/c from each other. Both concretes were assigned with different resistivity values since carbonated concrete has higher resistance due to pores filled with calcium carbonate. Resistivity values were set to 600 and 300 Ω cm for carbonated and noncarbonated concretes, respectively. These values were estimated from bulk concrete resistance measured by the galvanostatic impulse technique.

Two physical laws govern the current flow in the bulk concrete, first is the Laplace equation (Equation 7), which describes the potential distribution in concrete volume assuming charge conservation. The second one is Ohm's law (Equation 8), which determines the corrosion current density at a certain point in the concrete volume given the resistivity and electrical fields are known.[2,9,15,38-41] These two boundary conditions were set in carbonated and noncarbonated concretes.

$$\nabla . \boldsymbol{E} = 0, \tag{7}$$

$$\boldsymbol{I} = -\frac{1}{\rho}\nabla E, \tag{8}$$

TABLE 4 Corrosion parameters for active steel in carbonated concrete

Sample no.	Scan rate (mV/s)	Corrosion potential $E_{corr,a}$ (mV/SCE)	Corrosion current density $I_{corr,a}$ ($\mu A/cm^2$)	Anodic Tafel constant $\beta_{a,a}$ (mV/dec)	Cathodic Tafel constant $\beta_{c,a}$ (mV/dec)	Stern–Geary constant B (mV)
1	0.1	−653	0.622	200	265	49
2	0.1	−645	0.645	260	295	60
3	0.1	−702	0.300	250	220	51
4	0.1	−642	0.885	258	220	52
5	0.1	−652	0.510	230	240	51
6	0.1	−652	0.650	250	250	54
Average		−658	0.602	241	248	53
STD		20	0.175	21	26	4
7	0.5	−665	2.600	280	350	68
8	0.5	−662	0.898	256	240	54
9	0.5	−645	0.800	215	210	46
10	0.5	−641	1.000	225	230	49
11	0.5	−668	0.350	180	190	40
12	0.5	−676	1.280	275	309	63
Average		−659.5	1.155	239	255	53
STD		12	0.703	35	56	9
13	0.8	−660	1.244	272	298	62
14	0.8	−662	1.028	259	292	60
15	0.8	−658	0.550	230	230	50
16	0.8	−661	1.500	260	260	56
17	0.8	−543	0.600	280	250	57
18	0.8	−600	0.800	210	230	48
Average		−631	0.954	252	260	55
STD		45	0.342	24	27	5
Total Average		−649	0.903	244	254	54
Total STD		32	0.516	28	39	7
Partial polarization						
19	0.5	−601	0.600	-	210	-
20	0.5	−613	0.800	-	190	-
21	0.5	−692	0.900	-	220	-
22	0.5	−619	0.500	160	-	-
23	0.5	−598	0.900	250	-	-
24	0.5	−554	0.800	180	-	-
Average		−613	0.75	197	207	
STD		41	0.150	39	12	

TABLE 5 Corrosion parameters for passive steel in noncarbonated concrete

Sample no.	Scan rate (mV/s)	Corrosion potential $E_{corr,p}$ (mV/SCE)	Corrosion current density $I_{corr,p}$ ($\mu A/cm^2$)	Anodic Tafel constant $\beta_{a,p}$ (mV/dec)	Cathodic Tafel constant $\beta_{c,p}$ (mV/dec)	Stern–Geary constant B (mV)
1	0.1	−186	0.020	374	132	42
2	0.1	−261	0.068	700	145	52
3	0.1	−221	0.040	400	142	46
4	0.1	−244	0.053	700	118	44
5	0.1	−143	0.010	600	121	44
6	0.1	−300	0.037	700	120	44
Average		−226	0.038	579	130	45
STD		51	0.0193	140	11	3
7	0.5	−239	0.030	430	105	37
8	0.5	−253	0.070	650	150	53
9	0.5	−172	0.020	780	177	63
10	0.5	−218	0.080	650	140	50
11	0.5	−260	0.091	403	146	47
12	0.5	−318	0.150	500	160	53
Average		−243	0.073	569	146	50
STD		44	0.043	135	22	8
13	0.8	−223	0.055	560	110	40
14	0.8	−290	0.080	550	130	46
15	0.8	−267	0.080	400	110	37
16	0.8	−186	0.040	499	130	45
17	0.8	−214	0.030	350	180	52
18	0.8	−319	0.100	500	140	47
Average		−250	0.064	477	133	44
STD		46	0.025	77	24	5
Total Average		−240	0.0586	541	136	47
Total STD		48	0.034	129	21	6
Partial polarization						
19	0.5	−148	8.00E−03	-	140	-
20	0.5	−89	9.00E−03	-	150	-
21	0.5	−124	1.00E−02	-	110	-
22	0.5	−157	5.00E−03	700	-	-
23	0.5	−215	2.00E−03	1000	-	-
24	0.5	−137	5.00E−03	650	-	-
Average		−145	6.50E−03	783	133	-
STD		38	0.0028	154	17	-

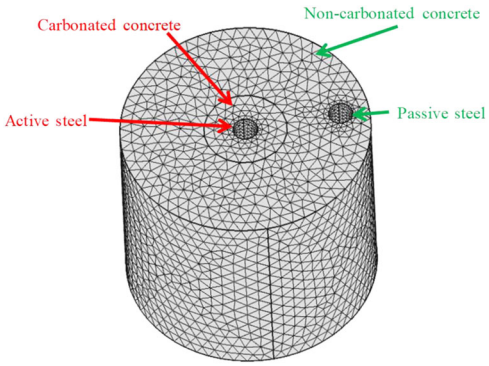

FIGURE 13 Sample geometry for numerical simulation of a macrocell corrosion system [Color figure can be viewed at wileyonlinelibrary.com]

where $\boldsymbol{I}$ is the local current density, ρ is the electrical resistivity of concrete, and E is the local value of the potential field.

The steel–concrete interface for both active and passive steel was modeled by the Butler–Volmer kinetics with their respective parameters, as presented in the following equations:

$$I_{\mathrm{corr,a}} = i_{\mathrm{corr,a}}\left(\exp\left(\frac{\log(10)\left(E_{\mathrm{a}} - E_{\mathrm{corr,a}}\right)}{\beta_{\mathrm{a,a}}}\right) - \exp\left(\frac{-\log(10)\left(E_{\mathrm{a}} - E_{\mathrm{corr,a}}\right)}{\beta_{\mathrm{c,a}}}\right)\right), \quad (9)$$

$$I_{\mathrm{corr,p}} = i_{\mathrm{corr,p}}\left(\exp\left(\frac{\log(10)\left(E_{\mathrm{p}} - E_{\mathrm{corr,p}}\right)}{\beta_{\mathrm{a,p}}}\right) - \exp\left(\frac{-\log(10)\left(E_{\mathrm{p}} - E_{\mathrm{corr,p}}\right)}{\beta_{\mathrm{c,p}}}\right)\right), \quad (10)$$

where, I_{a} and I_{p} are the corrosion currents following through the steel–concrete interface for active and passive steel, respectively. E_{a} and E_{p} are polarization potential for both steel rebars, respectively. Other parameters in the above equation are already obtained through the experimental study.

Boundary conditions for the periphery of the outer concrete cylinder and the top and bottom of both cylinders were set as *electrical insulation*. The interface between inner and outer concrete cylinders was set as *continuity*. That is, the current can flow from one cylinder to the other without interruption. The potential distribution and corrosion current densities were computed by solving Equation (7–10) numerically, with a selected range of corrosion parameters.

Table 6 presents the parameters set for the active and passive steel bars. Initially, the simulations were performed using the average values of each parameter obtained experimentally. Then their values were changed stepwise to cover the typical range reported in the literature. For this purpose, each parameter was assigned to a base value, which was the average value, and the parameter under study was varied. The effects of this variation were observed on the macrocell corrosion rate.

The simulations showed good convergence to a unique solution. Figures 14a and 14b show the potential and current distributions, respectively, in the concrete geometry. These distributions are coherent with the physical phenomena of galvanic corrosion of steel in concrete. When there is a short circuit between active and passive rebars, the active bars' potential shifts toward more positive values and the passive bar polarizes toward more negative potentials. Once the equilibrium is achieved, the potential on the active bar (E_{a}) and passive bar (E_{p}) could not reach the same value due to the ohmic drop caused by the resistance of the concrete between the two rebars. Higher corrosion densities were observed near both steel surfaces, whereas densities were reduced away from the steel rebars.

The macrocell corrosion current was recorded on the whole surface of steel rebars. Both active and passive steel showed similar values of macrocell current.

3.7 | Validation of macrocell current values

The normalized values of the macrocell corrosion current over the surface area were compared to two experimental studies carried out by the authors, presented elsewhere.[2,31] Sohail et al.[2] used similar geometry with active and passive steel rebars embedded in carbonated and noncarbonated coaxial cylinders, respectively. The macrocell corrosion current measured with an anode-to-cathode (a/d) ratio of 1, was compared with the numerical results from this study. On the other hand, Sohail et al.[21] had active steel rebar embedded in the chloride-contaminated concrete cylinder, whereas the passive bar (stainless steel), instead of being embedded in concrete, was placed in the water surrounding the concrete cylinder sample. The a/d ratio was also 1.

Figure 15 compares the macrocell corrosion current densities. In the first study, the macrocell current densities were between 0.50 and 1.94 $\mu A/cm^2$, with an average of 1.02 $\mu A/cm^2$ over three samples, whereas, in the second study, the macrocell current was between

TABLE 6 The electrochemical corrosion parameters used in the numerical simulation

	Active steel (anode) Carbonated concrete				Passive steel (cathode) Noncarbonated concrete			
Corrosion parameters		**Minimum**	**Base**	**Maximum**		**Minimum**	**Base**	**Maximum**
Concrete resistivity (Ω cm)	ρ	-	600	-	ρ	-	300	-
Corrosion rate (μA/cm²)	$I_{corr,a}$	0.1	0.85	2.6	$I_{corr,p}$	0.001	0.025	0.05
Corrosion potential (mV/SCE)	$E_{corr,a}$	−800	−650	−400	$E_{corr,p}$	−350	−200	50
Anodic Tafel slope (mV/dec)	$b_{a,a}$	350	245	30	$b_{a,p}$	350	550	1000
Cathodic Tafel slope (mV/dec)	$b_{c,a}$	100	260	350	$b_{c,p}$	60	150	220

Note: Value was set to base for each parameter when other parameters were studied.

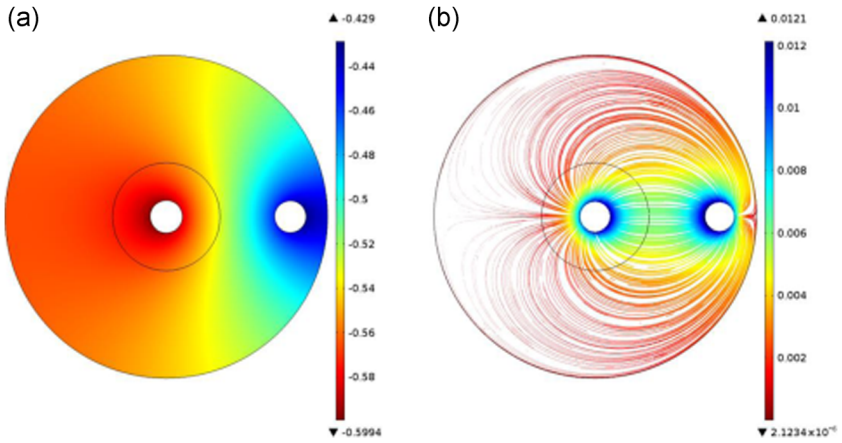

FIGURE 14 Macrocell corrosion system with active and passive steel in connection. (a) Corrosion potential in volts (V), and (b) corrosion current in amperes (A) [Color figure can be viewed at wileyonlinelibrary.com]

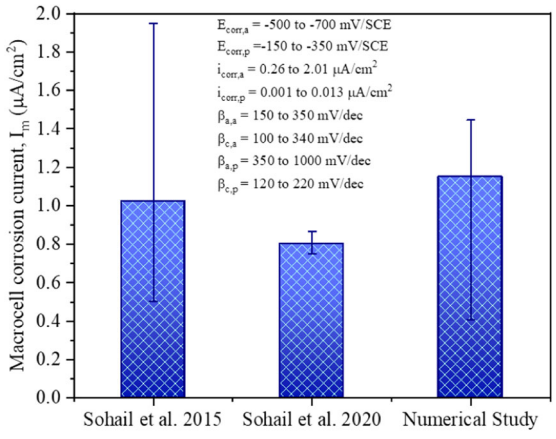

FIGURE 15 Comparison of macrocell corrosion current density with experimental studies of Sohail et al.[2,21] [Color figure can be viewed at wileyonlinelibrary.com]

0.75 and 0.86 μA/cm², over four samples with an average of 0.80 μA/cm². The numerically obtained macrocell current density was between 0.41 and 1.44 μA/cm². When the average values of all the parameters were used, the macrocell current was 1.15 μA/cm. Figure 15 also presents the range of parameters that yielded the macrocell current density within the range reported in the two studies.

With the variability generated by concrete conditions, corrosion products, and experimental conditions, it can be concluded that the corrosion parameters obtained from this study predicted the experimental results with reasonable accuracy.

4 | CONCLUSIONS AND RECOMMENDATIONS

Corrosion parameters in the partially carbonated concrete are reported through an extensive experimental study. The values used in literature to simulate the corrosion in reinforced concrete numerically are extracted either from chloride-contaminated concrete or from simulated concrete pore solution. The presented range of values are expected to increase the reliability in numerical modeling of the reinforcement corrosion. In addition, the estimations of ongoing corrosion rate through the LPR technique could be improved by using the presented range.

Following are some main conclusions of this study:

- The corrosion potential of active bars in carbonated concrete showed a range from −543 and −702 mV/SCE with an average value of −652 mV/SCE. The most frequent class was 650 mV/SCE over 24 samples. Passive steel in noncarbonated concrete showed a wider variability with values in the range from −143 to −319 mV/SCE, with an average of −240 mV/SCE. The most frequently occurring class on the histogram was 225 mV/SCE. The large variability could be attributed to the passivity range of steel rebars, where corrosion potential could be at different points based on oxygen availability, moisture, and temperature. However, the steel rebar would remain in a passive state with negligible corrosion current.
- Actively corroding rebars in carbonated concrete had a corrosion rate between 0.3 and 2.60 $\mu A/cm^2$, whereas, for passive steel in noncarbonated concrete, it was between 0.01 and 0.15 $\mu A/cm^2$.
- The anodic Tafel slope for the active steel bar was in the range of 180–280 mV/dec, whereas, for passive steel bars, it was between 350 and 1000 mV/dec. The cathodic Tafel slope constant was from 190 to 350 and 105 to 180 mV/dec for active and passive steels, respectively.
- The value of the Stern–Geary constant B for passive steel was 47 mV, which is close to the generally employed values in the LPR technique. However, for the actively corroding steel, the value was 54 mV, which was at least two times higher than the employed values to extract instantaneous current density by LPR.
- The numerical simulation of a galvanic corrosion system comprising active steel in carbonated and passive steel in noncarbonated concrete was performed. The results were compared to two experimental studies. It was observed that the obtained corrosion parameters predicted the macrocell corrosion rates on active steel rebars with reasonable accuracy.

ACKNOWLEDGMENTS

The authors are highly thankful to the Higher Education Commission (HEC) of Pakistan for providing scholarships for this study. Authors are also thankful for the Laboratoire Matériaux et Durabilité des Constructions (LMDC), INSA, UPS, Université de Toulouse, for making its facilities available to carry out the study. Open Access funding provided by the Qatar National Library.

DATA AVAILABILITY STATEMENT

The raw/processed data required to reproduce these findings cannot be shared at this time as the data also forms part of an ongoing study.

ORCID

Muazzam G. Sohail http://orcid.org/0000-0002-1826-2741

REFERENCES

[1] J. Broomfield, *Corrosion of Steel in Concrete, Understanding, Investigation and Repair*, 2nd ed., Taylor and Francis, London, UK **2007**.
[2] M. G. Sohail, S. Laurens, F. Deby, J. P. Balayssac, *Mater. Struct.* **2015**, *48*, 217.
[3] M. Otieno, H. Beushausen, M. Alexander, *Mater. Corros.* **2011**, *63*, 777.
[4] T. El Maaddawy, K. Soudki, *Cem. Concr. Compos.* **2007**, *29*, 168.
[5] S. Miyazato, N. Otsuki, *J. Adv. Concr. Technol.* **2010**, *8*, 135.
[6] J. Ge, O.b Isgor, *Mater. Corros.* **2007**, *58*, 573.
[7] A. Michel, M. Otieno, H. Stang, M. R. Geiker, *Cem. Concr. Compos.* **2016**, *70*, 171.
[8] S. Kranc, A. A. Sagüés, *Corros. Sci.* **2001**, *43*, 1355.
[9] J. Gulikers, M. Raupach, *Mater. Corros.* **2006**, *57*, 618.
[10] E. Redaelli, L. Bertolini, W. Peelen, R. Polder, *Mater. Corros.* **2006**, *57*, 628.
[11] M. G. Sohail, R. Kahraman, N. G. Ozerkan, N. A. Alnuaimi, B. Gencturk, M. Dawood, A. Belarbi, *J. Perform. Constr. Facil.* **2018**, *32*, 04018059.
[12] Z.-T. Chang, B. Cherry, M. Marosszeky, *Corros. Sci.* **2008**, *50*, 357.
[13] B. Elsener, *Corros. Sci.* **2005**, *47*, 3019.
[14] P. Garcés, M. C. Andrade, A. Saez, M. C. Alonso, *Corros. Sci.* **2005**, *47*, 289.
[15] J. Warkus, M. Brem, M. Raupach, *Mater. Corros.* **2006**, *57*, 636.
[16] C.-Y. Kim, J.-K. Kim, *Constr. Build. Mater.* **2008**, *22*, 1129.
[17] G. Song, *Cem. Concr. Compos.* **2000**, *22*, 407.
[18] M. Babaee, A. Castel, *Cem. Concr. Res.* **2016**, *88*, 96.
[19] F. Duprat, T. Larrard, N. T. Vu, *Mater. Corros.* **2019**, *70*, 1934.
[20] A. E. Poursaee, *Doctoral thesis*, University of Waterloo (Waterloo, Canada), **2007**.
[21] M. G. Sohail, R. Kahraman, N. A. Alnuaimi, B. Gencturk, W. Alnahhal, M. Dawood, A. Belarbi, *Constr. Build. Mater.* **2020**, *232*, 117205.
[22] C. Alonso, M. Castellote, C. Andrade, *Electrochim. Acta* **2002**, *47*, 3469.
[23] H. W. Song, C. H. Lee, K. Y. Ann, *Cem. Concr. Compos.* **2008**, *30*, 113.
[24] A. Nasser, *PhD Thesis,* University of Paul Sabatier, University of Toulouse III (Toulouse, France) **2010**.
[25] M. E. Ismail, H. R. Soleymani, *Can. J. Civil Eng.* **2002**, *29*, 863.
[26] ASTM C876-09, Test Method for Corrosion Potentials of Uncoated Reinforcing Steel in Concrete **2009**.
[27] R. Neves, F. Branco, J. de Brito, *Cem. Concr. Compos.* **2013**, *41*, 9.
[28] B. Elsener, C. Andrade, J. Gulikers, R. Polder, M. Raupach, *Mater. Struct.* **2003**, *36*, 461.
[29] L. Bertolini, B. Elsener, P. Pedeferri, R. B. Polder, *Corrosion of Steel in Concrete*, John Wiley & Sons, New York, NY **2004**.
[30] H. R. Soleymani, M. E. Ismail, *Cem. Concr. Res.* **2004**, *34*, 2037.

[31] M. G. Sohail, *Ph.D. Thesis,* Universite de Paul Sabatier, Universite de Toulouse III (Toulouse, France) **2013**.
[32] W. Nguyen, J. F. Duncan, T. M. Devine, C. P. Ostertag, *Electrochim. Acta* **2018**, *271*, 319.
[33] A. Nasser, A. Clément, S. Laurens, A. Castel, *Corros. Sci.* **2010**, *52*, 2878.
[34] C. Andrade, J. A. González, *Mater. Corros.* **1978**, *29*, 515.
[35] W. Nguyen, J. F. Duncan, T. M. Devine, C. P. Ostertag, *Electrochim. Acta* **2018**, *271*, 319.
[36] X. L. Zhang, Z. H. Jiang, Z. P. Yao, Y. Song, Z. D. Wu, *Corros. Sci.* **2009**, *51*, 581.
[37] I. Martínez, C. Andrade, *Mater. Corros.* **2011**, *62*, 932.
[38] A. Clément, S. Laurens, G. Arliguie, F. Deby, *Eur. J. Environ. Civil Eng.* **2012**, *16*, 491.
[39] M. Raupach, *Mater. Corros.* **2006**, *57*, 605.
[40] J. Gulikers, M. Raupach, *Mater. Corros.* **2006**, *57*, 603.
[41] C. Andrade, C. Alonso, *Mater. Struct.* **2004**, *37*, 623.

How to cite this article: M. G. Sohail, S. Laurens, F. Deby, J. P. Balayssac, N. Al Nuaimi. Electrochemical corrosion parameters for active and passive reinforcing steel in carbonated and sound concrete. *Materials and Corrosion*. 2021;72:1854–1871.
https://doi.org/10.1002/maco.202112569